Available online at website: https://journal.bcrec.id/index.php/bcrec

Bulletin of Chemical Reaction Engineering & Catalysis, 22 (1) 2027, 25-41

Original Research Article

Cooperative Mn–Cu Catalysis for Oxygen-Coupled Oxidative Decarboxylation: Kinetic and Mechanistic Insights

Setyo Yanus Sasongko[1,2], Tri Partono Adhi[1*], I.G.B. Ngurah Makertihartha[1], Afif Syaifuddin[2], Dinda Nailla Amoryna[2]

[1]Department of Chemical Engineering, Institut Teknologi Bandung, Bandung, 40132, Indonesia
[2]PT Aimtopindo Nuansa Kimia, Bandung, 40212, Indonesia.

Received: 16th October 2026; Revised: 28th October 2026; Accepted: 29th October 2026
Available online: 7th November 2026; Published regularly: April 2027

Abstract

Oxidative decarboxylation of fatty acids represents a promising hydrogen-free route for hydrocarbon production, yet catalytic systems operating under moderate aerobic conditions with kinetic and mechanistic validation remain limited. In this study, a biomimetic Mn–Cu catalytic system was evaluated for the oxidative decarboxylation of lauric acid at 110–150 °C under continuous air flow. Reaction performance was assessed through CO_2 evolution as a kinetically relevant indicator of carboxyl-group cleavage, enabling real-time evaluation of decarboxylation activity. The Mn–Cu system exhibited substantially higher catalytic activity than the corresponding monometallic Mn- and Cu-based systems, indicating cooperative interactions between the two metal components. Kinetic analysis showed that the reaction proceeded under an oxygen-coupled regime without an observable induction period. The initial CO_2 formation rate under air reached 0.1863 mmol min^{-1}, approximately 9.3 times higher than that under N_2, confirming the essential role of oxygen in sustaining catalytic turnover. Radical trapping experiments using butylated hydroxytoluene (BHT) resulted in concentration-dependent inhibition of CO_2 formation, reaching up to 73.3%, supporting the involvement of radical species in the decarboxylation pathway. GC–MS analysis confirmed hydrocarbon formation, with C_{11} compounds as the dominant fraction, consistent with lauric acid decarboxylation. A plausible Mn–Cu-assisted oxygen-coupled pathway is proposed, in which Cu contributes to oxygen activation while Mn facilitates carboxylate oxidation through electron-transfer processes. However, specific Cu–oxygen species, Mn oxidation states, and radical intermediates were not directly identified. Overall, these findings provide coherent kinetic and mechanistic evidence for Mn–Cu-assisted oxidative decarboxylation under moderate aerobic conditions.

Copyright © 2027 by Authors, Published by BCREC Publishing Group. This is an open access article under the CC BY-SA License (https://creativecommons.org/licenses/by-sa/4.0).

Keywords: Kinetic Analysis; Mn–Cu Catalyst; Oxidative Decarboxylation; Oxygen Activation; Radical Mechanism

How to Cite: Sasongko, S. Y., Adhi, T. P., Makertihartha, I. G. B. N., Syaifuddin, A., Amoryna, D. N. (2027). Cooperative Mn–Cu Catalysis for Oxygen-Coupled Oxidative Decarboxylation: Kinetic and Mechanistic Insights. *Bulletin of Chemical Reaction Engineering & Catalysis*, 22 (1), 25-41. (DOI: 10.9767/bcrec.20893)

Permalink/DOI: https://doi.org/10.9767/bcrec.20893

1. Introduction

Carboxylic acid decarboxylation is an important transformation in biomass conversion, particularly for converting fatty acids into hydrocarbon-based biofuels. This process involves the cleavage of the C–C bond between the carboxyl group (–COOH) and the β-carbon, resulting hydrocarbons containing one fewer carbon atom than the feed carboxylic acid, followed by the release of CO_2 as a byproduct [1–6]. In renewable fuel production, this reaction pathway offers a promising approach for converting fatty acids into hydrocarbons without requiring substantial amounts of external hydrogen, making it an attractive alternative to conventional hydroprocessing [1,2,7,8].

Previous studies have demonstrated that fatty acid deoxygenation through decarboxylation and decarbonylation can produce hydrocarbons within the liquid fuel range, including diesel and aviation fuel fractions [1,4,7,8]. However, many reported catalytic systems still require relatively severe operating conditions, such as temperatures

* Corresponding Author.
Email: tpadhi@itb.ac.id (T.P. Adhi)

above 300 °C, elevated hydrogen pressures, or metal catalysts such as Pt, Au, Pd, Ag, Co, and Ir [4,5,9–13]. Non-catalytic approaches, such as pyrolysis, have also been extensively investigated but generally produce broad product distributions and limited selectivity owing to the predominance of uncontrolled thermal reactions [9,14]. These limitations highlight the need to develop alternative catalytic systems capable of promoting C–C bond cleavage under milder operating conditions.

From a biochemical perspective, enzymatic oxidative decarboxylation represents a promising strategy for converting fatty acids under mild reaction conditions. Relevant examples include cytochrome P450 fatty acid decarboxylase from *Jeotgalicoccus* sp. and the non-heme iron-dependent enzymes UndA and UndB. These enzymatic systems demonstrate how metal-mediated oxidative chemistry can facilitate fatty acid conversion through reactive intermediate formation and radical-mediated pathways [15–18]. More broadly, biomimetic approaches inspired by enzymatic systems emphasize the importance of oxidant activation, reactive intermediate formation, and electron transfer through redox processes. In molecular oxygen (O_2)-based systems, oxygen activation at metal centers represents a potentially important step in generating reactive oxygen species and facilitating oxidative transformations [19].

Transition metals, such as Cu, Mn, and Fe, have been reported to activate O_2 and generate reactive oxygen species, including superoxide and peroxide species, which participate in various selective oxidation reactions [20–23]. Furthermore, studies in bioinorganic chemistry have demonstrated that cooperative interactions between metal centers can facilitate electron transfer, enhance redox-cycle efficiency, and sustain the formation of reactive oxidative intermediates [20,22,24–27]. Nevertheless, the application of cooperative redox systems to the oxidative decarboxylation of fatty acids, particularly in homogeneous catalytic systems operating under moderate aerobic conditions, remains relatively unexplored. Therefore, systematic investigations correlating oxygen availability, radical-scavenger inhibition, reaction kinetics, and product formation are needed to elucidate the underlying reaction mechanism and establish a more comprehensive understanding of cooperative transition-metal catalysis in the oxidative decarboxylation of fatty acids.

2. Materials and Methods

2.1 Materials

Lauric acid (analytical grade, ≥ 99.5%), dimethyl sulfoxide (DMSO, analytical grade, ≥99%), sodium hydroxide (NaOH, analytical grade, ≥ 99.5%), Mn (p.a., ≥ 98%) and Cu (p.a., ≥ 95%) salts used as catalyst and co-catalyst, n-hexane (p.a., ≥ 99%), and hydrochloric acid (HCl, 36%, p.a.) were supplied by Merck. All chemicals were used as received without further purification.

2.2. Oxidative Decarboxylation Reaction System

The oxidative decarboxylation reaction was conducted in a 250 mL glass reflux reactor operated in batch mode. The reactor was equipped with a gas inlet, a thermocouple, and a temperature controller with PID regulation (±5 °C accuracy). The reaction mixture consisted of 13 g of lauric acid, 100 mL of DMSO, 1 g of Mn catalyst, and 0.1 g of Cu co-catalyst (Mn : Cu = 10 : 1, w/w), which were introduced into the reactor. The reaction was carried out at various temperatures (110, 125, 135, and 150 °C). Once the desired temperature was reached, air was continuously introduced into the system at a flow rate of 1 L min^{-1}. The reaction was maintained for 3 h under these conditions. The evolved reaction gases were passed through two gas absorption bottles containing 100 mL of 0.4 N NaOH solution to capture the CO_2 generated during the reaction.

2.3. CO_2 Measurement and Kinetic Analysis

The CO_2 captured in the form of carbonate was quantified by volumetric analysis using a carbonate–bicarbonate titration method with standardized 0.01 N HCl solution. The resulting CO_2 amounts (mmol) were used to evaluate reaction performance and determine kinetic parameters, based on the Equation (1):

$$\text{R-COOH} \rightarrow \text{R-H} + CO_2 \qquad (1)$$

In this study, analysis was performed based on the temporal evolution of CO_2. CO_2 evolution was used as a sensitive kinetic probe to monitor carboxylate group cleavage in real time. Each primary decarboxylation event generates one molecule of CO_2; however, CO_2 evolution is used here as a kinetic descriptor rather than a direct measure of overall conversion. The 0–60 min interval was selected as the kinetic window because it exhibits a linear relationship between CO_2 evolution and time, representing differential kinetic conditions with minimal influence from mass transfer limitations or substrate depletion. The reaction rate (r) was defined as Equation (2):

$$r = \frac{d\left(n_{CO_2}\right)}{dt} \qquad (2)$$

where n_{CO_2} is the amount of CO_2 (mmol), and t is time (min).

The apparent rate constant (k_{app}) was calculated by normalizing the rate of CO_2

Copyright © 2027, ISSN 1978-2993

formation to the initial amount of lauric acid can be written as Equation (3) below:

$$k_{app} = r \frac{1}{n_{RCOOH,0}} \quad (3)$$

where $n_{RCOOH,0}$ is the initial amount of lauric acid (mmol), and k_{app} is expressed in min^{-1} (or s^{-1}).

In the initial stage of the reaction, substrate conversion remains low and oxygen is continuously supplied; therefore, its effective concentration can be considered approximately constant. Under these conditions, the system can be approximated using pseudo-first-order kinetics with respect to the substrate. Within this framework, the apparent rate constant (k_{app}) represents the overall kinetic parameter in the initial regime and should not be interpreted as an elementary rate constant

The apparent kinetic parameters were determined using the linearized Arrhenius equation:

$$\ln k_{app} = \ln A_{app} - \frac{E_{a,app}}{RT} \quad (4)$$

where A_{app} is the apparent pre-exponential factor (s^{-1}), $E_{a,app}$ is the apparent activation energy ($J.mol^{-1}$), R is the universal gas constant (8.3145 $J.mol^{-1}.K^{-1}$), and T is the absolute temperature (K).

2.4. Catalyst Reversibility Cycle Analysis

The analysis of cycle reversibility was performed based on the turnover number (TON) and turnover frequency (TOF). The TON is calculated from the total number of substrate molecules converted into products per active site of the catalyst before saturation or deactivation occurs [28], and can be calculated using Equation (5):

$$\text{TON} = \frac{\text{converted substrate (mmol)}}{\text{catalyst active site (mmol)}} \quad (5)$$

TOF, the catalytic cycle rate, is calculated from the number of TONs per reaction time [28], can be written as Equation (6):

$$TOF\ (h^{-1}) = \frac{TON}{reaction\ time} = \frac{converted\ substrate\ (mmol)}{catalyst\ active\ site\ (mmol) \times t\ (h)} \quad (6)$$

In this study, the turnover number (TON) and turnover frequency (TOF) are reported as apparent TON and apparent TOF, rather than intrinsic values based on the actual number of active sites. The apparent TON was determined based on the amount of CO_2 produced during the reaction, expressed as $TON_{CO_2,app}$. Meanwhile, the apparent TOF was expressed as $TOF_{0,app}$, calculated from the initial reaction rate (r_0) determined from the linear interval of 0–60 min.

2.5. Radical Scavenger Analysis

Radical scavenger experiments were conducted using the oxidative decarboxylation procedure described in Section 2.2, with the addition of BHT at 10%, 20%, and 30% (w/w) relative to the mass of the Mn catalyst. The reaction was performed at 125 °C for 3 h. The CO_2 produced was analyzed to evaluate the extent of radical inhibition. Radical inhibition was quantified by comparing the initial rate of CO_2 formation in the presence of BHT with that of the control system (without BHT), according to the Equation (7):

$$Inhibition = \frac{(r_{0,no\ BHT} - r_{0,BHT})}{r_{0,no\ BHT}} \times 100\% \quad (7)$$

where $r_{0,no\ BHT}$ is the initial CO_2 formation rate in the absence of BHT, and $r_{0,BHT}$ is the corresponding rate in the presence of BHT. BHT was introduced to assess the involvement of radical species in the reaction mechanism by monitoring changes in the initial CO_2 formation rate during the early stage of the reaction.

2.6. Product Analysis Using GC-MS

Liquid samples were analyzed using GC–MS (Shimadzu GCMS-QP2010 Plus) with an injection volume of 1.0 µL without dilution. Chromatographic separation was performed by gas chromatography and recorded as total ion chromatograms (TIC). Compound identification was carried out based on retention times and mass spectral matching against the NIST/Wiley library. Product distribution was determined semi-quantitatively based on peak area percentages (area%).

3. Results and Discussion

3.1. Cooperative Mn–Cu Catalytic Synergy

To evaluate whether oxidative decarboxylation proceeds via a cooperative mechanism or simply reflects additive contributions from individual metals, a direct comparison was conducted between monometallic systems (Mn and Cu) and the Mn–Cu bimetallic system under identical reaction conditions (125 °C, air flow rate of 1.0 $L.min^{-1}$). CO_2 evolution was monitored in real time and used as a direct indicator of carboxylate group cleavage, as well as a kinetic probe for the reaction.

As shown in Figure 1, both monometallic systems generated only limited amounts of CO_2 and rapidly reached a plateau at approximately 4–5 mmol after 180 min. In contrast, the Mn–Cu system exhibited significantly faster CO_2 formation from the initial stages of the reaction and continued to increase, reaching

Copyright © 2027, ISSN 1978-2993

approximately 18–19 mmol within the same time frame. This difference demonstrates that the Mn–Cu system exhibits significantly higher catalytic activity than the corresponding monometallic systems. During the initial reaction interval (0–60 min), the rate of CO_2 formation in the Mn–Cu system increased markedly, suggesting the presence of synergistic interactions between metal sites within the bimetallic catalyst. The negligible CO_2 formation observed in the absence of catalyst (Figure 1) confirms that solvent-derived or thermal contributions are not a dominant source of CO_2 under the studied conditions.

Quantitatively, the initial rate observed for the Mn–Cu system exceeds the sum of the individual contributions from the monometallic systems, indicating that the enhancement in activity is not simply additive. Rather, this behavior suggests the emergence of a more efficient catalytic pathway arising from the interaction between the two metal centers.

From a mechanistic perspective, this behavior is consistent with complementary functional roles of the metals, in which Cu facilitates oxygen activation, while Mn mediates carboxylate oxidation via a redox cycle. Such cooperation promotes more efficient electron transfer and sustains the generation of reactive intermediates throughout the reaction [25,29]. Overall, these results provide strong evidence that the enhanced activity of the Mn–Cu system originates from cooperative redox synergy between the two metal centers, enabling more efficient coupling of oxygen activation and C–C bond cleavage compared to monometallic systems.

3.2. Oxygen Dependence

The role of oxygen in the oxidative decarboxylation process was evaluated through control experiments by comparing aerobic (air) and inert (N_2) conditions under identical reaction parameters (125 °C, gas flow rate of 1.0 L.min^{-1}). CO_2 evolution was monitored in real time as a direct indicator of carboxylate group cleavage and as a kinetic probe of the reaction. As shown in Figure 2, the Mn–Cu system under an air atmosphere exhibited a rapid increase in CO_2 formation during the initial stages of the reaction, followed by a gradual approach to a plateau after approximately 120–150 min, reaching a total CO_2 yield of 12 mmol at 180 min. In contrast, under N_2 conditions, CO_2 formation was significantly suppressed, reaching only 2 mmol over the same time interval.

These results demonstrate that the presence of oxygen is essential for driving the reaction. The pronounced decrease in CO_2 formation under N_2

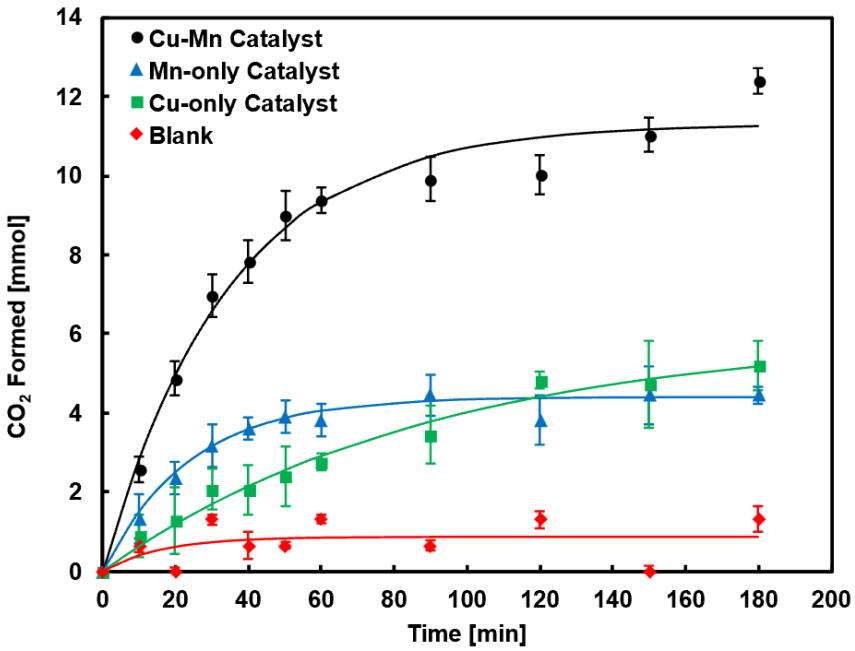


Figure 1. Time-resolved CO_2 evolution during oxidative decarboxylation of lauric acid ($C_{12}H_{24}O_2$) at 125 °C under air using Mn–Cu (10:1), Mn-only, Cu-only, and no-catalyst systems. Reaction conditions: 13 g substrate, 100 mL DMSO, total catalyst loading = 1.0 g, air flow = 1.0 L.min^{-1}, reaction time = 3 h. Negligible CO_2 formation in the absence of catalyst indicates that CO_2 evolution is primarily associated with catalytic oxidative decarboxylation rather than solvent decomposition or thermal background reactions. The circle (●) represent Cu-Mn catalayst, triangle (▲) represent Mn catalyst, square (■) represent Cu catalyst, diamond (◆) represent blank (no catalyst), and straight line (—) represent model. Error bars represent standard deviation from triplicate experiments (n = 3).

Copyright © 2027, ISSN 1978-2993

conditions indicates that the reaction is not governed by purely thermal pathways under the conditions employed. Furthermore, the data show that oxygen not only enhances the reaction rate but is also required to sustain the catalytic redox cycle. Under inert conditions, the regeneration of active species is hindered, leading to a rapid decline in catalytic activity after the initial stage.

From a mechanistic standpoint, this behavior is consistent with a pathway in which molecular oxygen is activated at the Cu center to generate reactive oxygen species, which subsequently mediate the oxidation of carboxylate groups via Mn. In the absence of oxygen, the formation of these reactive intermediates is suppressed, resulting in limited carboxylate radical generation and reduced CO_2 evolution. Overall, these findings indicate that C–C bond cleavage in the Mn–Cu system is strongly coupled to oxygen activation, which plays a critical role in sustaining the catalytic cycle through a cooperative redox mechanism.

Table 1. The initial rate (r_0) of CO_2 formation and the rate of increase in activity under different conditions.

Condition	r_0 [mmol.min^{-1}]	Ratio r_0 to N_2
Under air	0.1863	9.3106
Under N_2	0.0200	1.0000

The effect of oxygen on reaction kinetics was further analyzed by comparing the initial rate of CO_2 formation (r_0), determined from the slope of the linear region within 0–60 min (Figure 2). This approach enables evaluation of intrinsic catalytic activity while minimizing the influence of mass transport limitations and changes in reaction composition. As summarized in Table 1, the Mn–Cu system under an air atmosphere exhibited an initial rate of 0.1863 mmol.min^{-1}, whereas under N_2 conditions, the rate decreased to 0.0200 mmol min^{-1}, corresponding to an approximately 9.3-fold enhancement under aerobic conditions.

These results demonstrate that oxygen functions are not only as a reactant but also as a key factor governing the reaction rate by sustaining the catalytic redox cycle. Under aerobic conditions, the continuous supply of oxygen enables efficient regeneration of active sites, thereby maintaining a high reaction rate during the initial stages. In contrast, under inert conditions, the regeneration of active species is severely limited, leading to a pronounced decline in catalytic activity.

From a mechanistic perspective, the strong dependence on oxygen suggests that the rate-limiting step is associated with oxygen activation or electron transfer processes involving reactive oxygen species [30–32]. This behavior indicates

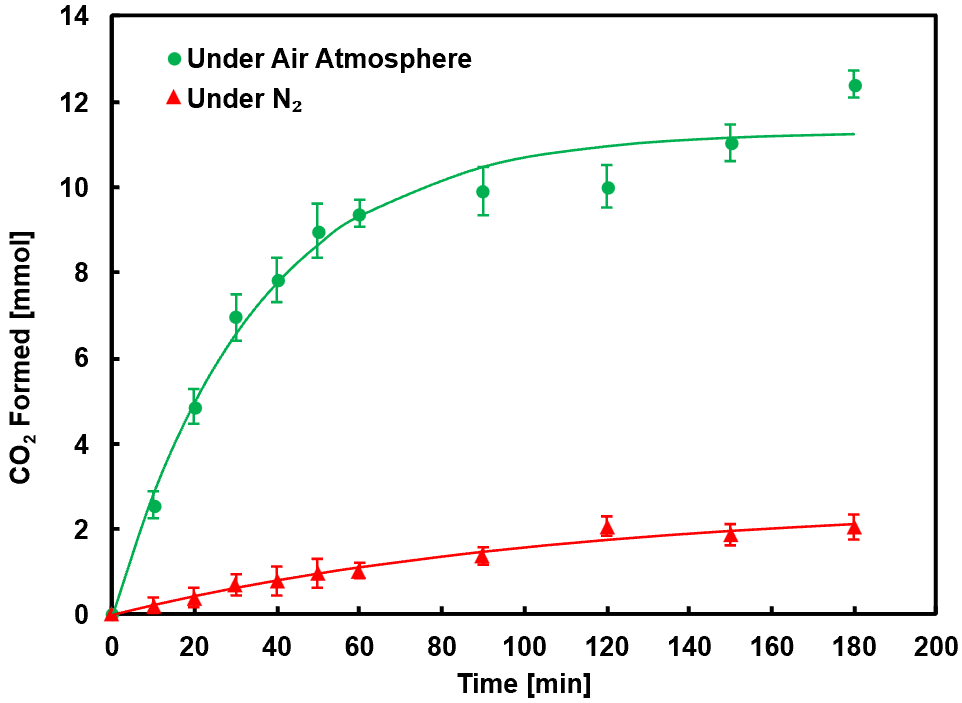


Figure 2. Effect of gas atmosphere on CO_2 evolution during oxidative decarboxylation of lauric acid at 125 °C using the Mn–Cu catalytic system (10:1 w/w). Reactions were performed under continuous air or N_2 flow (1.0 L.min^{-1}). Suppression of CO_2 formation under N_2 indicates the oxygen-dependent nature of the decarboxylation pathway. The circle (●) represent reaction under atmospheric air, triangle (▲) represent reaction under N_2 gas, and straight line (—) represent model. Error bars correspond to triplicate experiments (n = 3).

Copyright © 2027, ISSN 1978-2993

that oxygen plays a direct role in sustaining catalytic turnover through the continuous generation of reactive intermediates. These phenomenon support an oxygen-coupled kinetic regime, in which both the sustainability of the catalytic cycle and the observed reaction rate depend on the system's ability to continuously activate molecular oxygen.

3.3. Radical Trapping

To evaluate the involvement of radical intermediates in the oxidative decarboxylation mechanism, radical trapping experiments were conducted using butylated hydroxytoluene (BHT) as a scavenger. This approach complements the indirect evidence obtained from the reaction's oxygen dependence (Section 3.2) and its initial kinetic behavior (Section 3.4), both of which suggest the presence of a radical-mediated pathway. BHT, a phenolic antioxidant, efficiently intercepts free radicals via a hydrogen atom transfer (HAT) mechanism, thereby inhibiting radical chain propagation [33–36]. In these experiments, BHT was introduced into the reaction mixture prior to heating at a defined concentration relative to the catalyst, while all other reaction conditions were maintained identical to the standard system. CO_2 evolution was monitored as a direct indicator of carboxyl group cleavage, as described in Sections 3.2.

The effect of BHT addition on CO_2 evolution is presented in Figure 3. In the absence of a scavenger, CO_2 formation increased rapidly during the initial stages of the reaction, reflecting a high decarboxylation rate. In contrast, the addition of BHT resulted in a pronounced suppression of CO_2 formation, particularly in the early reaction phase. This inhibition of CO_2 formation indicates that the reactive species responsible for carboxylate cleavage can be effectively intercepted by BHT. Given that CO_2 evolution has been directly correlated with the decarboxylation step (Section 3.2), these findings provide strong evidence for the involvement of radical intermediates in the reaction pathway [36,37].

To evaluate the kinetic effects of BHT addition, the analysis focused on the initial reaction interval (0–60 min), corresponding to the linear region previously identified as the initial kinetic regime (Section 3.4). The results are presented in Figure 4. Increasing BHT concentration led to a systematic decrease in the slope of the CO_2 evolution curves, indicating a

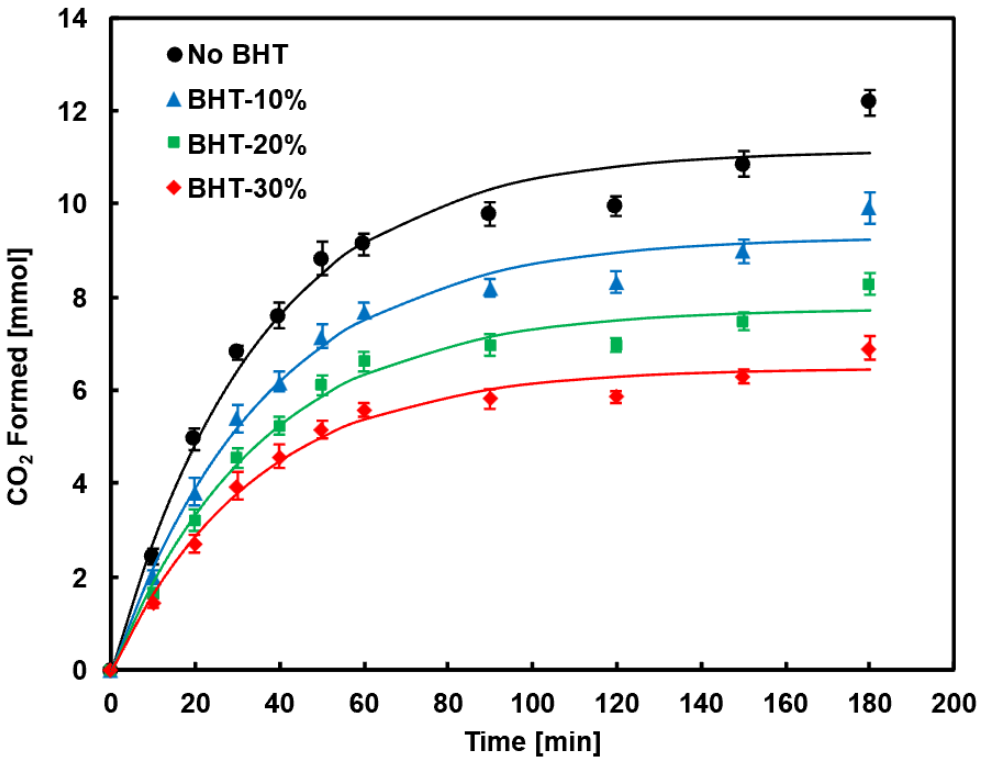


Figure 3. The effect of adding the radical scavenger BHT (10, 20, and 30 wt% relative to the Mn catalyst mass) on CO_2 evolution during the oxidative decarboxylation of lauric acid catalyzed by the Mn–Cu system. The presence of BHT significantly suppressed CO_2 formation, indicating that carbon radicals play a role in the early stages of the reaction and can be intercepted by BHT. The circle (●) represent no BHT, triangle (▲) represent 10% BHT, square (■) represent 20%, diamond (◆) represent 30% BHT (w/w of Mn catalyst) and straight line (—) represent model. Error bars represent standard deviation from triplicate experiments (n = 3).

Copyright © 2027, ISSN 1978-2993

reduction in the initial reaction rate (r_0). Since r_0 was determined from the same initial linear region used in the preceding kinetic analysis, these results directly correlate BHT-induced inhibition with disruption of the dominant reaction pathway during the early stages.

The quantitative results are summarized in Table 2. The addition of BHT led to a progressive decrease in the initial reaction rate (r_0), with inhibition reaching approximately 73% at the highest concentration. This trend demonstrates a clear dose-dependent inhibition, which is characteristic of radical-mediated reaction systems. The radical trapping results are consistent with previous evidence derived from oxygen dependence (Section 3.2), initial kinetic behavior (Section 3.3), and GC–MS product distributions (Section 3.7), which reveal the presence of species characteristic of radical pathways, such as alkenes and alcohols [38–40]. The pronounced decrease in CO_2 formation upon BHT addition provides direct experimental evidence that the decarboxylation step involves radical intermediates contributing to CO_2 generation. Collectively, these findings reinforce the interpretation that the reaction proceeds via an oxygen-coupled radical mechanism, as further illustrated in the mechanistic scheme presented in Section 3.8.

3.4. Kinetic Regime and Initial Rate Analysis

Reaction kinetics were analyzed using CO_2 evolution as a sensitive and kinetically relevant probe of carboxyl group cleavage, enabling quantitative evaluation of the reaction rate without the need for direct monitoring of

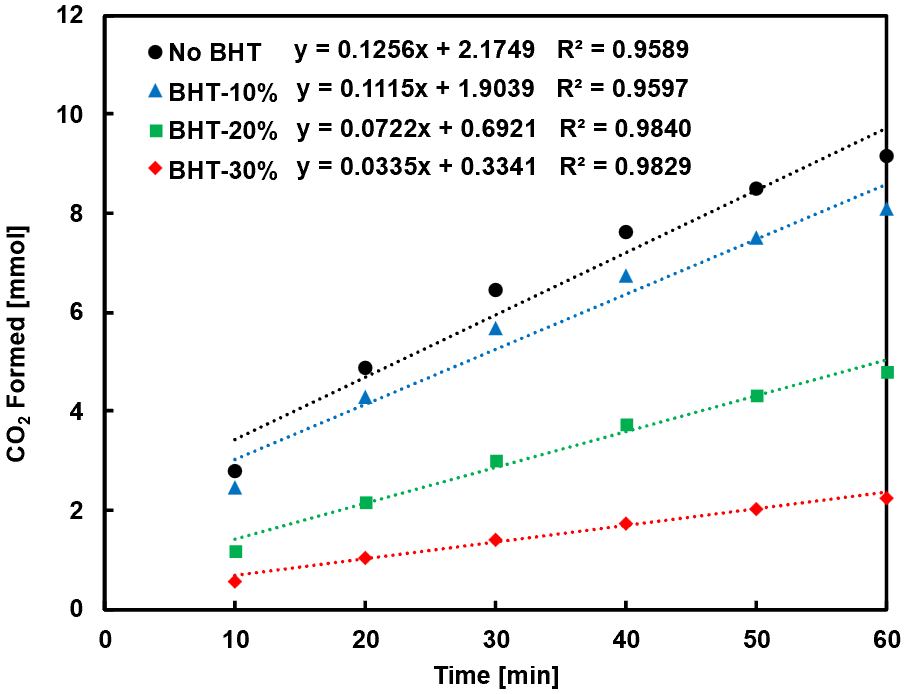


Figure 4. Evolution profile of CO_2 during the initial kinetic regime (0–60 minutes) for the Mn–Cu catalytic system with and without the addition of BHT (10–30 wt% relative to the Mn catalyst mass). Linear regression was used to determine the initial reaction rate (r_0) from the slope of the curve ($y = ax + b$). The gradual decrease in the slope value with increasing BHT concentration indicates reaction rate inhibition, providing kinetic evidence for the involvement of radical species in the oxidative decarboxylation mechanism.

Table 2. The effect of adding BHT as a radical scavenger on CO_2 formation and the initial reaction rate over the 0–60-minute interval in a Mn–Cu-catalyzed oxidative decarboxylation system. The $r_{0,BHT}$ value was calculated from the slope of the CO_2 evolution curve in the initial linear region, while the percentage inhibition was calculated relative to the system without BHT.

BHT Concentration [%wt of Mn catalyst]	CO_2 formed at t = 60 min [mmol]	$r_{0,BHT}$ [mmol.min^{-1}]	Inhibition (%)
0	11.09	0.1256	
10	9.86	0.1115	11.23
20	7.09	0.0722	42.52
30	2.25	0.0335	73.33

Copyright © 2027, ISSN 1978-2993

substrate consumption. In this study, CO_2 evolution serves as a kinetic descriptor of decarboxylation activity rather than a direct measure of overall substrate conversion. This approach provides a meaningful representation of catalytic performance in oxidative decarboxylation systems.

To obtain representative kinetic parameters, the analysis focused on the early stages of the reaction under aerobic conditions (Section 3.2), where the system operates within an oxygen-coupled kinetic regime. It should be emphasized that CO_2 evolution is employed in this study as a sensitive kinetic descriptor of decarboxylation activity rather than a direct measure of total substrate conversion [41,42]. While each decarboxylation event produces one molecule of CO_2, secondary pathways may also contribute to CO_2 formation. Therefore, CO_2 evolution provides a reliable basis for kinetic and mechanistic interpretation, but does not represent a complete carbon balance of the system. The CO_2 evolution profiles exhibited a linear relationship with time in the initial interval (0–60 min) across all tested temperatures. No observable induction period was detected, indicating that the catalytic system is active from the onset of the reaction.

Within this interval, substrate conversion remains low and oxygen is present in excess due to continuous supply; therefore, the oxygen concentration can be considered effectively constant. Under these conditions, the system can be approximated as following pseudo-first-order kinetics with respect to the substrate. Accordingly, the 0–60 min interval was selected as a differential regime for extracting the initial rate (r_0) and the apparent rate constant (k_{app}). The consistent linearity observed within this region confirms that the reaction proceeds under kinetically controlled conditions, thereby enabling quantitative correlation between reaction rates and the underlying mechanistic behavior.

As shown in Figure 5, CO_2 evolution during the initial stage of the reaction (0–60 min) exhibits a linear relationship with time, with a high coefficient of determination ($R^2 \approx 1$). This linearity indicates that the reaction rate remains essentially constant over this interval. Beyond this interval, the CO_2 evolution profile deviates from linearity, likely due to decreasing substrate concentration and/or changes in the dynamics of reactive intermediates within the system. Accordingly, the 0–60 min interval was selected as the kinetic window for extracting initial rate parameters.

Assuming that oxygen remains in excess due to continuous supply and that substrate conversion is minimal during the initial stage, the system can be approximated using pseudo-first-order kinetics with respect to the substrate. Within this framework, the apparent rate constant (k_{app}) represents the overall reaction rate in the initial regime and should not be interpreted as an elementary rate constant. No induction period was observed, indicating that the Mn–Cu catalytic system is active from the onset of the reaction and maintains stable activity throughout the initial kinetic window.

The initial reaction rate (r_0) was determined from the slope of the CO_2 evolution curve within the linear interval of 0–60 min and used as a

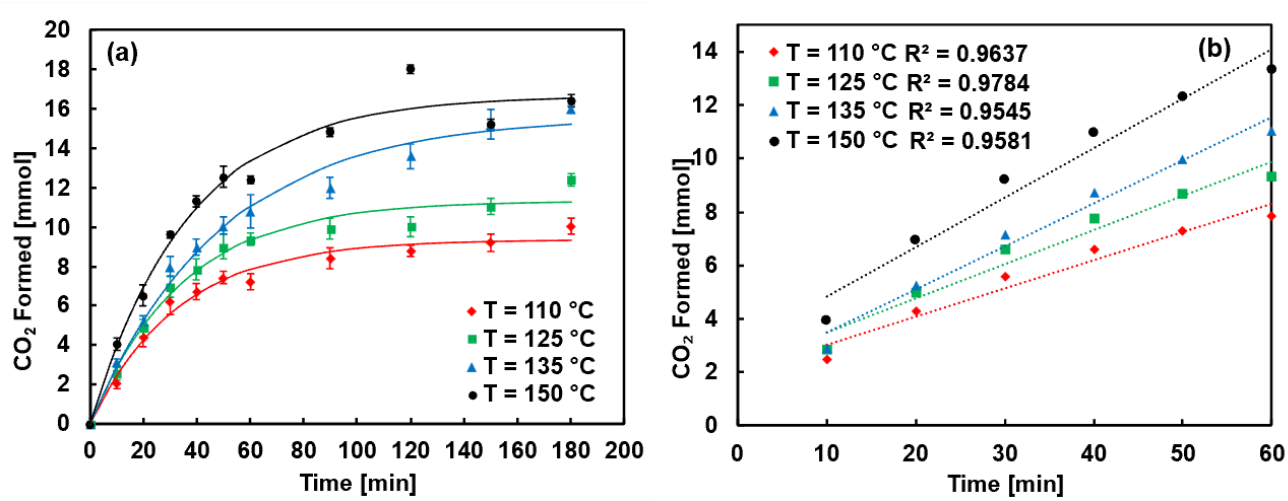


Figure 5. CO_2 formation during the initial phase of the reaction at various temperatures using a Mn–Cu catalytic system (mass ratio 10:1): (a) full-curved and (b) linear region (reaction time = 0-60 min). Reaction conditions: 13 g of substrate, 100 mL of DMSO, total catalyst 1.0 g, air flow rate 1.0 L.min^{-1}, reaction time 3 hours. The initial rate (r_0) was calculated from the linear region. The diamond (◆) represent CO_2 formed at reaction temperature 110 °C, square (■) represent at 125 °C, triangle (▲) represent at 135 °C, circle (●) represent at 150 °C, and straight line (—) represent model. Error bars represent standard deviation from triplicate experiments (n = 3).

Copyright © 2027, ISSN 1978-2993

quantitative parameter to compare catalytic activity across the different systems. The results show that the Mn–Cu system exhibits a significantly higher initial rate than the monometallic systems (Mn-only and Cu-only). Notably, the observed r_0 value exceeds the sum of the individual contributions from the monometallic systems, indicating that the enhancement in activity is not additive.

This behavior suggests the presence of synergistic interactions between metal sites in the bimetallic system, which enhance the efficiency of redox processes during the reaction [7]. This observation is consistent with the findings in Section 3.1, where the Mn–Cu system demonstrated a non-additive increase in CO_2 evolution. Overall, the initial rate analysis provides a quantitative basis for concluding that the combination of Mn and Cu results in a more active catalytic system than either component alone.

3.5. Temperature Dependence and Activation Energy

The initial reaction rates (r_0) for the Mn–Cu, Mn-only, and Cu-only systems are summarized in Table 3 to quantitatively assess the presence of catalytic synergy. The Mn–Cu system exhibits a higher initial rate than both monometallic systems. Notably, the observed r_0 value exceeds the sum of the individual contributions from the Mn-only and Cu-only systems, indicating that the enhancement in activity is not additive.

The Mn–Cu system exhibits an approximately 2.3-fold increase in the initial rate relative to the Mn-only system and a 3.5-fold increase relative to the Cu-only system. These enhancements indicate that the combined system outperforms each individual component. This non-additive behavior suggests the presence of synergistic interactions between metal sites, which enhance overall reaction efficiency. This observation is consistent with the results presented in Sections 3.1, 3.2, and 3.4, where increased CO_2 evolution and higher initial rates were observed for the Mn–Cu system. Overall, this kinetic analysis provides quantitative evidence that the Mn–Cu system exhibits superior catalytic activity compared to monometallic systems, likely arising from cooperative interactions within the redox cycle.

The effect of temperature on reaction kinetics was evaluated by measuring the initial rate (r_0) and the apparent rate constant (k_{app}) over a temperature range of 110–150 °C (Table 4). The results show that both r_0 and k_{app} increase systematically with increasing temperature. For example, the initial rate (r_0) increased from 0.1572 mmol.min^{-1} at 110 °C to 0.2648 mmol.min^{-1} at 150 °C, while the apparent rate constant (k_{app}) increased from 4.06×10^{-5} s^{-1} to 6.83×10^{-5} s^{-1}. This trend indicates that increasing temperature consistently enhances the reaction rate. As shown in Figure 6, the apparent rate constant (k_{app}) increases monotonically with increasing temperature. This behavior indicates that the reaction rate is sensitive to temperature within the studied range. The observed trend suggests that the system operates within a kinetically controlled regime governed by an activation process, thereby enabling further analysis using the Arrhenius approach [43,44].

The pseudo-activation energy of the oxidative decarboxylation reaction was determined via Arrhenius analysis by plotting $\ln(k_{app})$ against $1/T$ (Figure 7). The resulting Arrhenius plot exhibits a strong linear relationship, indicating that the reaction follows thermally activated kinetic behavior within the investigated temperature range. A comparison with literature data (Table 5) shows that thermal

Table 3. Initial rate (r_0) and relative increase in catalytic activity.

Catalyst	r_0 [mmol.min^{-1}]	r_0 to Mn Catalyst Ratio	r_0 to Cu Catalyst Ratio
Mn-based	0.0822	1.0000	1.5433
Cu-based	0.0533	0.6480	1.0000
Mn-Cu	0.1863	2.2655	3.4963

Table 4. Initial rate (r_0) and the value of k_{app} at various reaction temperatures.

Temperature [°C]	r_0 [mmol.min^{-1}]	k_{app} [min^{-1}]	k_{app} [s^{-1}]
110	0.1572	0.0024	4.06×10^{-5}
125	0.1863	0.0029	4.81×10^{-5}
135	0.2136	0.0033	5.51×10^{-5}
150	0.2648	0.0041	6.83×10^{-5}

Copyright © 2027, ISSN 1978-2993

decarboxylation of fatty acids typically requires high activation energies (≥ 200 kJ.mol^{-1}) and operates at temperatures above 400 °C. In metal-based heterogeneous catalytic systems, reported activation energies generally fall within the range of 90–150 kJ.mol^{-1}, often accompanied by relatively high operating temperatures (≥ 250 °C). In contrast, the Mn–Cu system investigated in this study exhibits a substantially lower apparent activation energy (~17.6 kJ.mol^{-1}) and operates effectively under moderate aerobic conditions (110–150 °C).

This substantial difference indicates that the reaction pathway is not governed by purely thermal C–C bond cleavage but instead proceeds via a catalytic pathway involving oxygen activation and the formation of reactive intermediates. In this context, the low activation energy is more consistent with a mechanism involving electron transfer and/or radical intermediates sustained by a catalytic redox cycle, rather than conventional thermal pathways. This interpretation is supported by the strong dependence of the reaction on oxygen (Section 3.2) and the absence of an induction period during the early stages (Section 3.5.4), indicating that the catalytic system is active from the onset and capable of sustaining activity under the applied conditions. The interplay between oxygen activation, regeneration of active species, and kinetic stability suggests that the reaction rate is governed by the dynamics of the catalytic cycle rather than solely by thermal energy input.

Table 5. Comparison of activation energy values with various sources in the literature.

System	Catalyst	Operation Temperature [°C]	Activation Energy, E_a [kJ.mol^{-1}]	Kinetic Method	Ref
Thermal deoxygenation/ pyrolysis of oleic acid	Non-catalytic	400-600	275.3	TGA, Coats-Redfern	[14]
PFAD thermal deoxygenation	Heterogeneous	350-500	210-240	TGA	[45]
PFAD deoxygenation over Ni/Co-zeolite	Heterogeneous	300-450	120-150	TGA	[45]
Stearic acid over Co/NaX zeolite	Heterogeneous	260-300	93.5	Batch kinetics	[13]
Fatty acid decarboxylation over Ni/C	Homogeneous (metal non-catalytic)	300-370	n.a.	Conversion vs T	[46]
Photodecarboxy-lation of acyl hypoiodites	Homogeneous	25-60	n.a.	Isothermal k	[47]
Fatty acid decarboxylation over Cu-Mn catalyst system	Biomimetic-homogeneous	110-150	17.57	Actual kinetic (CO_2 probe)	This study

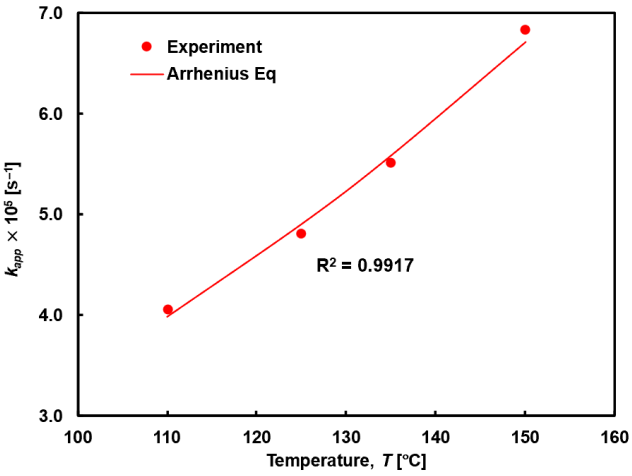


Figure 6. Correlation between the k_{app} coefficient and temperature. Circle (●) represent experimental data and straight line (—) represent data fitting form Arrhenius equation.

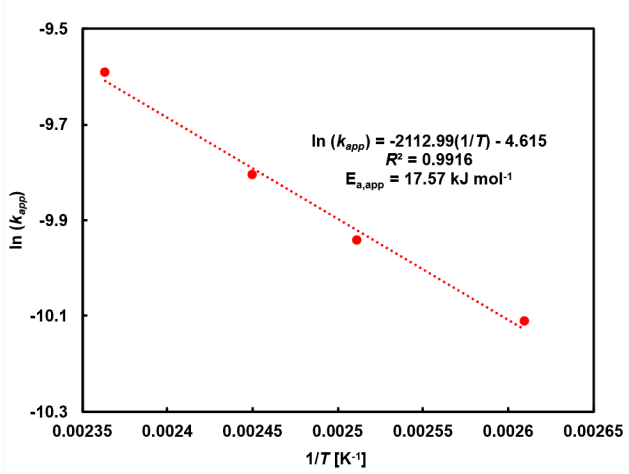


Figure 7. Arrhenius plot for oxidative decarboxylation of lauric acid catalyzed by Mn–Cu (10:1 w/w) under air. Apparent rates constant (k_{app}) were determined at 110, 125, 135, and 150 °C from the linear region of CO_2 evolution (0–60 min). The apparent activation energy ($E_{a,app}$) was calculated from the slope of ln(k_{app}) vs 1/T.

Copyright © 2027, ISSN 1978-2993

Although activation energy values reported in the literature were obtained using different kinetic methodologies, this comparison highlights that the Mn–Cu system provides a reaction pathway with significantly lower energy barriers than thermal decarboxylation and most previously reported catalytic systems. The low apparent activation energy suggests that the rate-limiting step is associated with oxygen activation or electron transfer rather than direct C–C bond cleavage. These findings show that oxidative decarboxylation in the Mn–Cu system proceeds via an oxygen-coupled kinetic pathway mediated by a cooperative redox cycle, enabling efficient conversion under moderate aerobic conditions.

3.6. Catalytic Efficiency: Apparent TON and TOF

To evaluate the catalytic efficiency of the Mn–Cu system, the CO_2-based turnover number ($TON_{CO_2,app}$) and initial turnover frequency ($TOF_{0,app}$) were determined, as shown in Figure 8. These parameters characterize the number of catalytic cycles and the turnover rate during the initial stage of the reaction. $TON_{CO_2,app}$ is defined as the ratio of the moles of CO_2 formed to the total moles of catalytic metal, while $TOF_{0,app}$ is calculated by normalizing the initial reaction rate to the number of catalytic metal sites. The results show that $TON_{CO_2,app}$ increases with increasing temperature, indicating that the system sustains catalytic activity throughout the reaction. This trend is accompanied by an increase in $TOF_{0,app}$, consistent with the temperature dependence of the apparent rate constant obtained from Arrhenius analysis.

Importantly, no significant decrease in $TOF_{0,app}$ was observed during the initial reaction stage across the studied temperature range. This indicates the absence of rapid catalyst deactivation within the initial kinetic window and suggests that the Mn–Cu system possesses sufficient redox stability to support repeated catalytic cycles. These observations are consistent with the absence of an induction period and the stable kinetic behavior discussed in Section 3.4.

To contextualize the observed catalytic performance, the TON and TOF values were compared with those reported for several transition metal-based homogeneous decarboxylation systems in the literature (Table 6). Most of these systems operate at elevated temperatures (190–280 °C) under inert (N_2)

Table 6. Comparison of TON and TOF values with various sources in the literature (*Calculated by authors).

Catalyst	System	Reaction Condition	TON*	TOF* [h^{-1}]	Ref
$PdCl_2$	Homogeneous catalytic	280 °C/under N_2	< 10	< 3	[48]
$(Ph_3P)_2PdCl_2$	Homogeneous catalytic	250 °C/under N_2	~10	~10	[49]
$(Me_2PhP)_2Rh(CO)Cl$	Homogeneous catalytic	250 °C/under N_2	710	130	[49]
$IrCl(CO)(PPh_3)_2$	Homogeneous catalytic	160 °C/under N_2	20	4	[50]
$Ni(OAc)_2$	Homogeneous catalytic	190 °C/under N_2	< 9	< 0.6	[51]
$FeCl_2$	Homogeneous catalytic	190 °C/under N_2	<10	<3.3	[52]
Mn(II)-Cu(II)	Biomimetic-homogeneous	150 °C/under atmospheric air	14.8	29.6	This study

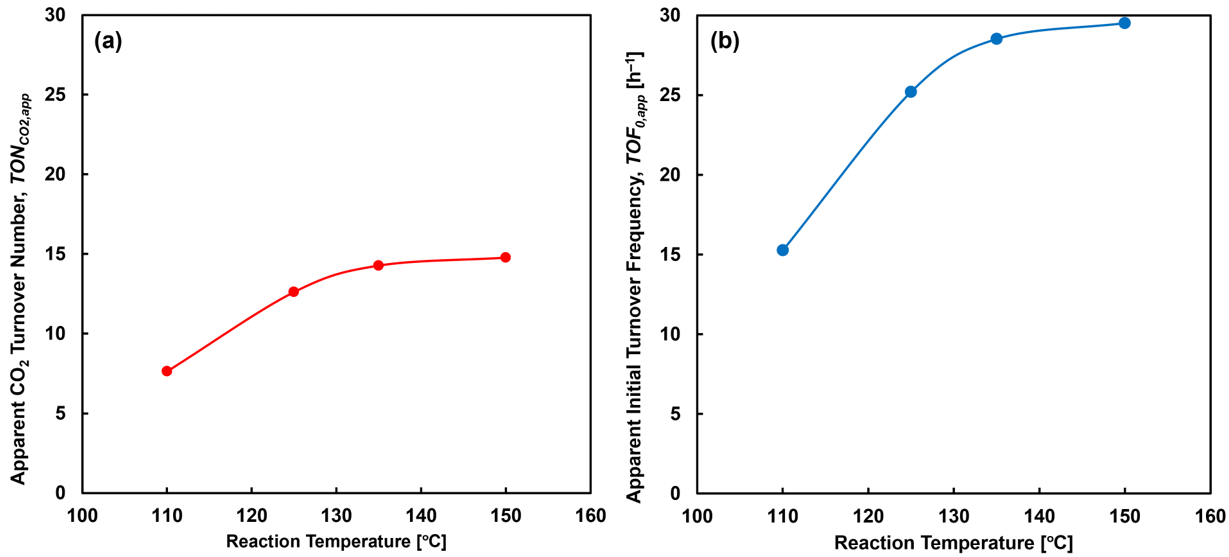


Figure 8. Correlation between the k_{app} coefficient and temperature. Circle (●) represent experimental data and straight line (—) represent data fitting form Arrhenius equation.

Copyright © 2027, ISSN 1978-2993

conditions and, in some cases, exhibit higher TON and TOF values. In contrast, the Mn–Cu system investigated in this study operates under more moderateconditions (110–150 °C, air atmosphere), achieving a $TON_{CO_2,app}$ of 14.8 and a $TOF_{0,app}$, of 29.6 h^{-1}. Under these conditions, these values demonstrate that the system is capable of sustaining catalytic activity in a relatively mild operating regime.

This distinction highlights that the Mn–Cu system enables oxidative decarboxylation at significantly lower temperatures compared to most reported systems. This observation is consistent with the activation energy analysis (Section 3.5.5), which indicates a reduced energy barrier for the reaction. Overall, the $TON_{CO_2,app}$ and $TOF_{0,app}$, analyses demonstrate that the Mn–Cu system maintains catalytic activity under moderate aerobic conditions, supporting the hypothesis that the reaction proceeds via a redox cycle coupled with oxygen activation. It should be noted, however, that these CO_2-based metrics reflect the extent of decarboxylation rather than the distribution of final products. Therefore, molecular-level characterization using GC–MS is required to establish a direct link between CO_2 evolution and the underlying chemical transformation pathways.

3.7. Product Distribution

Although CO_2 evolution provides a direct indicator of carboxyl group cleavage, molecular-level product identification is essential to confirm the underlying transformation pathways. Therefore, GC–MS analysis was performed to evaluate the product distribution and its relationship to the proposed radical-mediated oxidative decarboxylation mechanism, thereby providing strong molecular evidence supporting the correlation between CO_2 evolution and hydrocarbon formation.

The distribution is mainly centered within the C_8–C_{12} range, indicating selective formation of liquid fuel-range hydrocarbons (Table 7, Figure 9). Minor fractions of C_{13}–C_{16} suggest secondary reactions such as radical recombination, while the presence of C_6 indicates limited chain scission processes. The product distribution was evaluated semi-quantitatively based on GC–MS peak area normalization. This approach provides reliable comparative trends in product selectivity but does not represent absolute product yields. Nevertheless, the predominance of C_{11} hydrocarbons offers direct molecular-level evidence supporting the decarboxylation pathway ($C_{12} \rightarrow C_{11}$), consistent with the observed CO_2 evolution. In addition to the dominant C_{11} product, the formation of the C_6–C_{10} fraction (6.2%) indicates the occurrence of secondary radical fragmentation via β-scission [18,46,53]. However, the predominance of the C_{11} fraction suggests that this fragmentation pathway is not primary, but rather a secondary process following the formation of the initial alkyl radical.

The product distribution also includes a notable fraction of alkenes, indicating that radical termination occurs not only via hydrogen abstraction but also through elimination pathways. The presence of these alkenes is consistent with radical-mediated systems, in which alkyl radicals may undergo dehydrogenation prior to final stabilization. Importantly, the detection of oxygenated compounds such as alcohols and ketones provides evidence that molecular oxygen participates not

Table 7. Product distribution based on carbon content.

Carbon Number	Major Product Type(s)	GC Area (%)
C_6	Cyclohexanone	0.04
C_8	Octane, octane	1.35
C_9	Nonane, nonadiene	3.25
C_{10}	Decane, decene,	1.56
C_{11}	Undecane, undecadiene	89.2
C_{12}	Dodecane	3.66
C_{13}–C_{16}	Alkene	0.53
Total		99.59

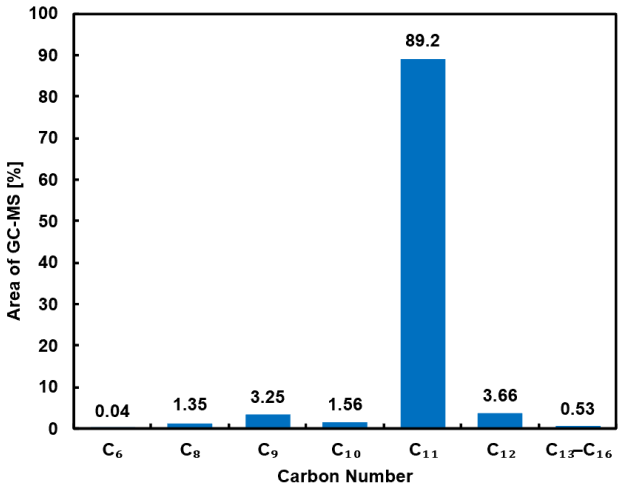


Figure 9. Carbon number distribution of hydrocarbon products obtained from GC–MS analysis. The product spectrum is dominated by the C_{11} fraction (89.2%), corresponding to the primary decarboxylation product of lauric acid ($C_{12} \rightarrow C_{11}$). The distribution is mainly centered within the C_8–C_{12} range, indicating selective formation of liquid fuel-range hydrocarbons. Minor fractions of C_{13}–C_{16} suggest secondary reactions such as radical recombination, while the presence of C_6 indicates limited chain scission processes.

Copyright © 2027, ISSN 1978-2993

only in the initiation step but also in radical termination through the formation of peroxy intermediates (ROO•) [38,39]. This observation supports an oxygen-coupled radical mechanism, consistent with the strong oxygen dependence of the reaction (Section 3.2).

Minor amounts of C_{12} products (3.66%) are attributed to non-decarboxylative secondary pathways, likely involving the transformation of oxygenated intermediates or hydrogen transfer processes. Meanwhile, the presence of higher-carbon products (C_{13}–C_{16}) in trace quantities likely arises from secondary reactions such as radical recombination or rearrangement, although their contribution to the primary pathway is negligible. Overall, the GC–MS product distribution is in strong agreement with the proposed radical-mediated oxidative decarboxylation mechanism. The predominance of C_{11} products provides direct confirmation of the primary reaction pathway, while the presence of fragmentation and oxygenated products reflects a secondary reaction network coupled with oxygen activation. Collectively, these results not only complement the CO_2-based kinetic analysis but also reinforce the mechanistic model in which the Mn–Cu system facilitates oxidative decarboxylation via a controlled radical pathway driven by oxygen activation.

3.8. Mechanistic Implications of the Mn–Cu System

The combined experimental results suggest that oxidative decarboxylation of lauric acid over the Mn–Cu catalytic system proceeds through an oxygen-coupled and redox-mediated pathway. This interpretation is supported by several key observations: the higher CO_2 evolution rate over the Mn–Cu system compared with the corresponding monometallic Mn- and Cu-based systems, the strong suppression of CO_2 formation under N_2, the concentration-dependent inhibition by BHT, and the predominance of C_{11} hydrocarbons in the GC–MS product distribution. The enhanced activity of the Mn–Cu system indicates that the two metal components do not act independently. Instead, their combination appears to create a more effective redox environment for promoting carboxylate activation and C–C bond cleavage. The comparison between air and N_2 further shows that molecular oxygen plays an essential role in sustaining the reaction. Under air, the initial rate of CO_2 formation was markedly higher than under N_2, indicating that oxygen is involved not only as an oxidant but also as a key component in maintaining catalytic turnover.

Based on these findings, Cu is proposed to contribute to oxygen activation, while Mn is proposed to assist carboxylate oxidation through electron-transfer processes. However, the specific identities of the Cu–oxygen species, Mn oxidation states, and metal–carboxylate intermediates were not directly determined in this study. Therefore, these roles should be interpreted as mechanistic possibilities consistent with the observed kinetic behavior, rather than as fully resolved elementary steps. A plausible pathway involves initial activation of the carboxylate species within the Mn–Cu redox environment, followed by one-electron oxidation to generate a carboxyl radical or radical-like intermediate. This intermediate can undergo decarboxylation to release CO_2 and form an alkyl radical. The resulting alkyl radical may then be converted into hydrocarbons through hydrogen abstraction, elimination, or secondary radical reactions. The predominance of C_{11} products in the GC–MS analysis supports lauric acid decarboxylation as the main pathway, whereas the presence of C_8–C_9 and minor C_{13}–C_{15} fractions indicates that secondary fragmentation and recombination reactions may also occur.

The radical-trapping experiment provides additional support for this interpretation. The addition of BHT caused a concentration-dependent decrease in CO_2 formation and initial reaction rate, indicating that radical species participate in the decarboxylation pathway. Nevertheless, because the radical intermediates were not directly detected, the BHT results should be regarded as strong kinetic evidence for radical involvement rather than definitive identification of specific radical species.

Overall, the Mn–Cu system appears to promote oxidative decarboxylation through the coupling of oxygen activation, redox-mediated carboxylate oxidation, and radical-based product formation. The proposed pathway is consistent with the kinetic, inhibition, oxygen-dependence, and GC–MS evidence obtained in this study. Further spectroscopic investigations, such as EPR spin trapping, in situ UV–Vis, or XPS analysis, are required to directly identify the reactive oxygen species, metal oxidation states, and radical intermediates involved in the catalytic cycle.

4. Conclusions

This study demonstrates that the Mn–Cu biomimetic catalytic system effectively promotes the oxidative decarboxylation of lauric acid under moderate aerobic conditions. The Mn–Cu system exhibited higher CO_2 evolution than the corresponding monometallic Mn- and Cu-based systems, indicating a cooperative catalytic effect between the two metal components. The negligible CO_2 formation in catalyst-free experiments confirms that CO_2 evolution primarily originates from the catalytic process

Copyright © 2027, ISSN 1978-2993

rather than background thermal or solvent-derived reactions. Kinetic analysis revealed an initial linear reaction regime without an observable induction period, while the substantially higher initial CO_2 formation rate under air than under N_2 highlights the essential role of molecular oxygen in sustaining catalytic activity. Furthermore, the low apparent activation energy and concentration-dependent inhibition by BHT provide evidence supporting an oxygen-dependent, redox-mediated reaction pathway involving radical species. GC–MS analysis showed that the liquid products were predominantly hydrocarbons in the C_8–C_{15} range, with C_{11} as the major fraction, consistent with lauric acid decarboxylation as the principal transformation pathway.

Collectively, these study support a plausible Mn–Cu-assisted mechanism involving molecular oxygen activation, redox-mediated carboxylate oxidation, and radical participation in hydrocarbon formation. Nevertheless, the specific identities of the reactive oxygen species, copper and manganese intermediates, and metal–carboxylate complexes remain unresolved. Therefore, the proposed mechanism should be regarded as an interpretation supported by kinetic, oxygen-dependence, radical inhibition, and product characterization results rather than a fully established sequence of elementary reactions. This study also establishes an experimental framework for investigating oxidative decarboxylation by integrating real-time CO_2 evolution as a kinetic probe with molecular-level product analysis. These investigations will be essential to validate the proposed mechanism and evaluate the potential of Mn–Cu catalytic systems for the sustainable production of biomass-derived hydrocarbons.

Acknowledgements

The authors gratefully acknowledge the support from the Department of Chemical Engineering, Institut Teknologi Bandung, for providing research facilities and academic guidance. The authors also thank PT Aimtopindo Nuansa Kimia for technical support during experimental work.

Conflict of Interest

The authors declare no conflict of interest.

Declaration of Generative AI Use

During the preparation of this manuscript, the authors used ChatGPT AI to check the language and improve the readability of the text. After using this tool, the authors reviewed and edited the content and take full responsibility for the entire content of the published article.

CRediT Author Statement

Author Contributions: S. Y. Sasongko: Conceptualization, Methodology, Investigation, Writing–original draft, Visualization; T. P. Adhi: Conceptualization, Supervision, Validation, Writing–review & editing; I. G. B. N. Makertihartha: Conceptualization, Supervision, Validation, Writing–review & editing; A. Syaifuddin: Investigation, Resources, Data curation, and Formal Analysis; D. N. Amoryna: Project Administration, Writing–review and editing, and Visualization. All authors have read and agreed to the published version of the manuscript.

References

[1] Santillan-jimenez, E., Crocker, M. (2012). Catalytic deoxygenation of fatty acids and their derivatives to hydrocarbon fuels via decarboxylation/decarbonylation. *J. Chem. Technol. Biotechnol.*, 87(8), 1041–1050. DOI: 10.1002/jctb.3775.

[2] Tabandeh, M., Cheng, C.K., Centi, G., Show, P.L., Chen, W.-H., Ling, T.C., Ong, H.C., Ng, E.-P., Juan, J.C., Lam, S.S. (2022). Recent advancement in deoxygenation of fatty acids via homogeneous catalysis for biofuel production. *Molecular Catalysis*, 523, 111207. DOI: https://doi.org/10.1016/j.mcat.2020.111207.

[3] Santner, P., Nahuel, S., Petrovai, N., Vig, F., Kara, S., Engin, B. (2023). Biocatalytic conversion of fatty acids into drop-in biofuels : Towards sustainable energy sources. *EFB Bioeconomy Journal*, 3, 100049. DOI: 10.1016/j.bioeco.2023.100049.

[4] Pikoli, S., Kunene, A., Makhubela, B.C.E. (2025). Enhanced ketonic decarboxylation of fatty acids using vanadia-modified nickel on zirconia catalysts. *Sustainable Energy and Fuels*, 9(10), 2738–2752. DOI: 10.1039/d4se01836b.

[5] Yeh, T.M., Hockstad, R.L., Linic, S., Savage, P.E. (2015). Hydrothermal decarboxylation of unsaturated fatty acids over PtSnx/C catalysts. *Fuel*, 156, 219–224. DOI: 10.1016/j.fuel.2015.04.039.

[6] Westenberg, R., Peralta-Yahya, P. (2023). Toward implementation of carbon-conservation networks in nonmodel organisms. *Current Opinion in Biotechnology*, 81, 102949. DOI: 10.1016/j.copbio.2023.102949.

[7] Kiméné, A., Wojcieszak, R., Paul, S., Dumeignil, F. (2018). Catalytic decarboxylation of fatty acids to hydrocarbons over non-noble metal catalysts: the state of the art. *Journal of Chemical Technology and Biotechnology*, 94(3), 658–669. DOI: 10.1002/jctb.5776.

Copyright © 2027, ISSN 1978-2993

[8] Gosselink, R.W., Hollak, S.A.W., Chang, S.-W., van Haveren, J., de Jong, K.P., Bitter, J.H., van Es, D.S. (2013). Reaction Pathways for the Deoxygenation of Vegetable Oils and Related Model Compounds. *ChemSusChem*, 6(9), 1576–1594. DOI: 10.1002/cssc.201300370.

[9] Miao, C., Marin-Flores, O., Davidson, S.D., Li, T., Dong, T., Gao, D., Wang, Y., Garcia-Pérez, M., Chen, S. (2016). Hydrothermal catalytic deoxygenation of palmitic acid over nickel catalyst. *Fuel*, 166, 302–308. DOI: 10.1016/j.fuel.2015.10.120.

[10] Arroyo, M., Briones, L., Hernando, H., Escola, J.M., Serrano, D.P. (2021). Selective decarboxylation of fatty acids catalyzed by Pd-supported hierarchical ZSM-5 zeolite. *Energy and Fuels*, 35(21), 17167–17181. DOI: 10.1021/acs.energyfuels.1c01373.

[11] Doll, K.M., Moser, B.R., Gerhard, K. (2021). Decarboxylation of oleic acid using iridium catalysis to form products of increased aromatic content compared to ruthenium systems. *International Journal of Sustainable Engineering*, 14(6), 2018–2024. DOI: 10.1080/19397038.2021.1978589.

[12] Monteiro, R.R.C., Dos Santos, I.A., Arcanjo, M.R.A., Cavalcante, C.L., de Luna, F.M.T., Fernandez-Lafuente, R., Vieira, R.S. (2022). Production of Jet Biofuels by Catalytic Hydroprocessing of Esters and Fatty Acids: A Review. *Catalysts*, 12(2), 1–24. DOI: 10.3390/catal12020237.

[13] Crawford, J.M., Smoljan, C.S., Lucero, J., Carreon, M.A. (2019). Deoxygenation of Stearic Acid over Cobalt-Based NaX Zeolite Catalysts. *Catalysts*, 9(42), 1–15. DOI: 10.3390/catal9010042.

[14] Asomaning, J., Mussone, P., Bressler, D.C. (2014). Thermal deoxygenation and pyrolysis of oleic acid. *Journal of Analytical and Applied Pyrolysis*, 105, 1–7. DOI: 10.1016/j.jaap.2013.09.005.

[15] Grant, J.L., Hsieh, C.H., Makris, T.M. (2015). Decarboxylation of fatty acids to terminal alkenes by cytochrome P450 compound i. *Journal of the American Chemical Society*, 137(15), 4940–4943. DOI: 10.1021/jacs.5b01965.

[16] Hsieh, C.H., Huang, X., Amaya, J.A., Rutland, C.D., Keys, C.L., Groves, J.T., Austin, R.N., Makris, T.M. (2017). The Enigmatic P450 Decarboxylase OleT Is Capable of, but Evolved To Frustrate, Oxygen Rebound Chemistry. *Biochemistry*, 56(26), 3347–3357. DOI: 10.1021/acs.biochem.7b00338.

[17] Zhang, S., Liu, Y. (2019). Mechanism of fatty acid decarboxylation catalyzed by a non-heme iron oxidase (UndA): A QM/MM study. *Organic and Biomolecular Chemistry*, 17(45), 9808–9818. DOI: 10.1039/c9ob02116g.

[18] Rude, M.A., Baron, T.S., Brubaker, S., Alibhai, M., Del Cardayre, S.B., Schirmer, A. (2011). Terminal olefin (1-alkene) biosynthesis by a novel p450 fatty acid decarboxylase from Jeotgalicoccus species. *Applied and Environmental Microbiology*, 77(5), 1718–1727. DOI: 10.1128/AEM.02580-10.

[19] Banerjee, R., Proshlyakov, Y., Lipscomb, J.D., Proshlyakov, D.A. (2015). Structure of the key species in the enzymatic oxidation of methane to methanol. *Nature*, 518(7539), 431–434. DOI: 10.1038/nature14160.

[20] Sahu, S., Goldberg, D.P. (2016). Activation of Dioxygen by Iron and Manganese Complexes: A Heme and Nonheme Perspective. *Journal of the American Chemical Society*, 138(36), 11410–11428. DOI: 10.1021/jacs.6b05251.

[21] Solomon, E.I., Goudarzi, S., Sutherlin, K.D. (2016). O2 Activation by Non-Heme Iron Enzymes. *Biochemistry*, 55(46), 6363–6374. DOI: 10.1021/acs.biochem.6b00635.

[22] Yee, G.M., Tolman, W.B. (2015). Transition metal complexes and the activation of dioxygen. *Metal Ions in Life Sciences*, 15, 131–204. DOI: 10.1007/978-3-319-12415-5_5.

[23] Liu, J.J., Diaz, D.E., Quist, D.A., Karlin, K.D. (2016). Copper(I)-Dioxygen Adducts and Copper Enzyme Mechanisms. *ISR J. Chem.*, (56), 9–10. DOI: 10.1002/ijch.201600025.

[24] Zúñiga, O.M., Mendoza, A., Cruz-Ramírez, M., Ramírez-Palma, L.G., Rebolledo-Chávez, J.P.F., Ortiz-Frade, L. (2025). Electrochemical and Spectroelectrochemical Studies on Oxygen Reduction Mediated by Cu(II) Complexes Containing the Alkylamine Ligand N,N-Dimethylethylendiamine. *Catalysts*, 15, 951, DOI: 10.3390/catal15100951.

[25] Bhowmick, S., Alam, S., Shah, A.K., Qureshi, M. (2021). Bimetallic cyclic redox couple in dimanganese copper oxide supported by nickel borate for boosted alkaline electrocatalytic oxygen evolution reaction. *Sustainable Energy and Fuels*, 5(9), 2517–2527. DOI: 10.1039/d1se00162k.

[26] Anxolabéhère-Mallart, E., Banse, F., Fave, C. (2026). O2 reductive activation using molecular Fe and Mn complexes: Reaction intermediates and reactivity. *Coordination Chemistry Reviews*, 562, 217907. DOI: 10.1016/j.ccr.2026.217907.

[27] Wang, C., Xiao, J. (2025). Activation of Molecular Oxygen and Selective Oxidation with Metal Complexes. *Accounts of Chemical Research*, 58(5), 714–731. DOI: 10.1021/acs.accounts.4c00731.

[28] Kozuch, S., Martin, J.M.L. (2012). "Turning Over" Definitions in Catalytic Cycles. *ACS Catalysis*, 2(12), 2787–2794. DOI: 10.1021/cs3005264.

Copyright © 2027, ISSN 1978-2993

[29] Chen, Q.-F., Xiao, Y., Hua, K., Zhang, H.-T., Zhang, M.-T. (2025). Bimetallic synergy in oxygen reduction: how tailored metal–metal interactions amplify cooperative catalysis. *Journal of the American Chemical Society*, 147(17), 14504–14518. DOI: 10.1021/jacs.5c01406.

[30] Guan, R., Bennett, E.L., Huang, Z., Xiao, J. (2022). Decarboxylative oxygenation of carboxylic acids with O2 via a non-heme manganese catalyst. *Green Chemistry*, 24(7), 2946–2952. DOI: 10.1039/d1gc04603a.

[31] Veljković, V.B., Savić, D.S., Lazić, M.L., Vrvić, M.M. (1999). Oxygen mass transfer requirements during ferrous iron oxidation by Thiobacillus ferrooxidans under controlled pH conditions. In: Amils, R., Ballester, A.B.T.-P.M. (eds) *Biohydrometallurgy and the Environment Toward the Mining of the 21 Century - Proceedings of the International Biohydrometallurgy Symposium*. Elsevier, pp. 617–623. DOI: 10.1016/S1572-4409(99)80063-7.

[32] Santillan-jimenez, E., Crocker, M. (2012). Catalytic deoxygenation of fatty acids and their derivatives to hydrocarbon fuels via decarboxylation/decarbonylation. *J. Chem. Technol. Biotechnol.*, 87(8), 1041–1050. DOI: 10.1002/jctb.3775.

[33] Tabandeh, M., Cheng, C.K., Centi, G., Show, P.L., Chen, W.-H., Ling, T.C., Ong, H.C., Ng, E.-P., Juan, J.C., Lam, S.S. (2022). Recent advancement in deoxygenation of fatty acids via homogeneous catalysis for biofuel production. *Molecular Catalysis*, 523, 111207. DOI: 10.1016/j.mcat.2020.111207.

[34] Santner, P., Nahuel, S., Petrovai, N., Vig, F., Kara, S., Engin, B. (2023). Biocatalytic conversion of fatty acids into drop-in biofuels : Towards sustainable energy sources. *EFB Bioeconomy Journal*, 3, 100049. DOI: 10.1016/j.bioeco.2023.100049.

[35] Pikoli, S., Kunene, A., Makhubela, B.C.E. (2025). Enhanced ketonic decarboxylation of fatty acids using vanadia-modified nickel on zirconia catalysts. *Sustainable Energy and Fuels*, 9(10), 2738–2752. DOI: 10.1039/d4se01836b.

[36] Yeh, T.M., Hockstad, R.L., Linic, S., Savage, P.E. (2015). Hydrothermal decarboxylation of unsaturated fatty acids over PtSnx/C catalysts. *Fuel*, 156, 219–224. DOI: 10.1016/j.fuel.2015.04.039.

[37] Westenberg, R., Peralta-Yahya, P. (2023). Toward implementation of carbon-conservation networks in nonmodel organisms. *Current Opinion in Biotechnology*, 81, 102949. DOI: 10.1016/j.copbio.2023.102949.

[38] Kiméné, A., Wojcieszak, R., Paul, S., Dumeignil, F. (2018). Catalytic decarboxylation of fatty acids to hydrocarbons over non-noble metal catalysts: the state of the art. *Journal of Chemical Technology and Biotechnology*, 94(3), 658–669. DOI: 10.1002/jctb.5776.

[39] Gosselink, R.W., Hollak, S.A.W., Chang, S.-W., van Haveren, J., de Jong, K.P., Bitter, J.H., van Es, D.S. (2013). Reaction Pathways for the Deoxygenation of Vegetable Oils and Related Model Compounds. *ChemSusChem*, 6(9), 1576–1594. DOI: 10.1002/cssc.201300370.

[40] Miao, C., Marin-Flores, O., Davidson, S.D., Li, T., Dong, T., Gao, D., Wang, Y., Garcia-Pérez, M., Chen, S. (2016). Hydrothermal catalytic deoxygenation of palmitic acid over nickel catalyst. *Fuel*, 166, 302–308. DOI: 10.1016/j.fuel.2015.10.120.

[41] Arroyo, M., Briones, L., Hernando, H., Escola, J.M., Serrano, D.P. (2021). Selective decarboxylation of fatty acids catalyzed by Pd-supported hierarchical ZSM-5 zeolite. *Energy and Fuels*, 35(21), 17167–17181. DOI: 10.1021/acs.energyfuels.1c01373.

[42] Doll, K.M., Moser, B.R., Gerhard, K. (2021). Decarboxylation of oleic acid using iridium catalysis to form products of increased aromatic content compared to ruthenium systems. *International Journal of Sustainable Engineering*, 14(6), 2018–2024. DOI: 10.1080/19397038.2021.1978589.

[43] Monteiro, R.R.C., Dos Santos, I.A., Arcanjo, M.R.A., Cavalcante, C.L., de Luna, F.M.T., Fernandez-Lafuente, R., Vieira, R.S. (2022). Production of Jet Biofuels by Catalytic Hydroprocessing of Esters and Fatty Acids: A Review. *Catalysts*, 12(2), 1–24. DOI: 10.3390/catal12020237.

[44] Crawford, J.M., Smoljan, C.S., Lucero, J., Carreon, M.A. (2019). Deoxygenation of Stearic Acid over Cobalt-Based NaX Zeolite Catalysts. *Catalysts*, 9(42), 1–15. DOI: 10.3390/catal9010042.

[45] Asomaning, J., Mussone, P., Bressler, D.C. (2014). Thermal deoxygenation and pyrolysis of oleic acid. *Journal of Analytical and Applied Pyrolysis*, 105, 1–7. DOI: 10.1016/j.jaap.2013.09.005.

[46] Grant, J.L., Hsieh, C.H., Makris, T.M. (2015). Decarboxylation of fatty acids to terminal alkenes by cytochrome P450 compound i. *Journal of the American Chemical Society*, 137(15), 4940–4943. DOI: 10.1021/jacs.5b01965.

[47] Hsieh, C.H., Huang, X., Amaya, J.A., Rutland, C.D., Keys, C.L., Groves, J.T., Austin, R.N., Makris, T.M. (2017). The Enigmatic P450 Decarboxylase OleT Is Capable of, but Evolved To Frustrate, Oxygen Rebound Chemistry. *Biochemistry*, 56(26), 3347–3357. DOI: 10.1021/acs.biochem.7b00338.

[48] Zhang, S., Liu, Y. (2019). Mechanism of fatty acid decarboxylation catalyzed by a non-heme iron oxidase (UndA): A QM/MM study. *Organic and Biomolecular Chemistry*, 17(45), 9808–9818. DOI: 10.1039/c9ob02116g.

Copyright © 2027, ISSN 1978-2993

[49] Miller, J.A., Nelson, J.A., Byrne, M.P. (1993). A highly catalytic and selective conversion of carboxylic acids to 1-alkenes of one less carbon atom. *The Journal of Organic Chemistry*, 58(1), 18–20. DOI: 10.1021/jo00053a008.

[50] Maetani, S., Fukuyama, T., Suzuki, N., Ishihara, D., Ryu, I. (2011). Efficient Iridium-Catalyzed Decarbonylation Reaction of Aliphatic Carboxylic Acids Leading to Internal or Terminal Alkenes. *Organometallics*, 30(6), 1389–1394. DOI: 10.1021/om1009268.

[51] John, A., Hillmyer, M.A., Tolman, W.B. (2017). Anhydride-Additive-Free Nickel-Catalyzed Deoxygenation of Carboxylic Acids to Olefins. *Organometallics*, 36(3), 506–509. DOI: 10.1021/acs.organomet.6b00940.

[52] Maetani, S., Fukuyama, T., Suzuki, N., Ishihara, D., Ryu, I. (2012). Iron-catalyzed decarbonylation reaction of aliphatic carboxylic acids leading to α-olefins. *Chemical Communications*, 48(19), 2552–2554. DOI: 10.1039/c2cc18093f.

[53] Bian, J., Wang, Y., Zhang, Q., Fang, X., Feng, L., Li, C. (2017). Fatty acid decarboxylation reaction kinetics and pathway of co-conversion with amino acid on supported iron oxide catalysts. *RSC Advances*, 7(75), 47279–47287. DOI: 10.1039/c7ra08507a

Copyright © 2027, ISSN 1978-2993